Graphene cover-promoted metal-catalyzed reactions

Yunxi Yao[a,b], Qiang Fu[a,1], Y. Y. Zhang[c], Xuefei Weng[d], Huan Li[d], Mingshu Chen[d], Li Jin[a], Aiyi Dong[a], Rentao Mu[a], Peng Jiang[a], Li Liu[b,e], Hendrik Bluhm[f], Zhi Liu[g], S. B. Zhang[c], and Xinhe Bao[a]

[a]State Key Laboratory of Catalysis, Dalian Institute of Chemical Physics, Chinese Academy of Sciences, Dalian 116023, People's Republic of China; [b]Department of Chemistry, Texas A&M University, College Station, TX 77843; [c]Department of Physics, Applied Physics, and Astronomy, Rensselaer Polytechnic Institute, Troy, NY 12180; [d]State Key Laboratory of Physical Chemistry of Solid Surfaces, Department of Chemistry, Xiamen University, Xiamen 361005, Fujian, People's Republic of China; [e]Department of Materials Science and Engineering, Texas A&M University, College Station, TX 77843; and [f]Chemical Sciences Division and [g]Advanced Light Source, Lawrence Berkeley National Laboratory, Berkeley, CA 94720

Edited by Alexis T. Bell, University of California, Berkeley, CA, and approved October 24, 2014 (received for review August 26, 2014)

Graphitic overlayers on metals have commonly been considered as inhibitors for surface reactions due to their chemical inertness and physical blockage of surface active sites. In this work, however, we find that surface reactions, for instance, CO adsorption/desorption and CO oxidation, can take place on Pt(111) surface covered by monolayer graphene sheets. Surface science measurements combined with density functional calculations show that the graphene overlayer weakens the strong interaction between CO and Pt and, consequently, facilitates the CO oxidation with lower apparent activation energy. These results suggest that interfaces between graphitic overlayers and metal surfaces act as 2D confined nanoreactors, in which catalytic reactions are promoted. The finding contrasts with the conventional knowledge that graphitic carbon poisons a catalyst surface but opens up an avenue to enhance catalytic performance through coating of metal catalysts with controlled graphitic covers.

graphene | interface catalysis | confinement effect | CO oxidation | platinum

Carbonaceous deposits such as carbidic carbon and graphitic carbon often form on transition metal (TM) surfaces in catalytic processes involving carbon-containing reactants (1). It has been shown that carbidic species can be involved in some hydrogenation reactions, which are attributed to the observed high reaction activity (2–5). In contrast, graphitic carbon deposited on TM is conventionally considered as catalyst poison due to its chemical inertness and physical blockage of surface active sites (6–8). It has been generally assumed that formation of graphitic carbon on metal catalysts should be avoided before and during catalytic reactions (9, 10). Nevertheless, for decades, extensive research efforts have been made to use surface carbon layers formed on TMs and to understand their role in catalytic reactions (11–14), which, however, have been impeded by complexity of the ill-defined carbon structures. Graphene, as a simple form of graphitic deposit, has been grown on many late TM surfaces via catalytic cracking of carbon-containing gases (15–20). Surface science studies on the well-defined graphene/metal surfaces have shown that gaseous molecules such as CO, O_2, and H_2O can be readily intercalated under the graphene overlayers (21–27). Defects in graphene including island edges (22, 23, 28–30), domain boundaries (26, 31, 32), and wrinkles (33) provide channels for molecule diffusion into the graphene/metal interfaces. These new results raise the intriguing possibility that the space between graphene overlayers and metal substrates can act as a 2D container for reactions. The distance between the graphene overlayers and the metal surfaces typically falls in the subnanometer range (19, 20), and molecules trapped inside interact directly with both the graphene cover and the metal substrate. Catalytic reactions, if occurring, are strongly confined in the 2D space, and extraordinary catalytic performance may be expected due to the confinement effect. In the present work, graphene/Pt(111) [Gr/Pt(111)] was used as the model system to test the hypothesis of 2D nanoreactor under graphene cover. In situ and near ambient-pressure surface science studies confirm that CO adsorption/desorption and CO oxidation reactions occur on Pt surface regions covered by monolayer graphene sheets. We show that the graphene overlayer weakens the CO adsorption on Pt, which alleviates the well-known CO poisoning effect. Consequently, CO oxidation within the confined space presents lower apparent activation energy compared with the open Pt surface. The result is contrasting with the traditional assumption that surface reactions on metals are blocked by graphitic overlayers, but rather opens a door to tailor the catalytic performance of metal catalysts through the surface decoration with graphitic nanostructures.

Results and Discussion

Graphene was grown on Pt(111) by exposing the Pt surface to 10^{-7} Torr ethylene (C_2H_4) at 950 K (23). Snapshots of in situ low-energy electron microscopy (LEEM) movie for the graphene growth show that the graphene coverage can be controlled by varying the ethylene exposure time (Fig. S1). Ethylene exposure with less than 10 min produces submonolayer graphene, which consists of monolayer graphene islands with the lateral size of micrometer or even smaller. These islands grow and merge together to form a full monolayer graphene upon extended ethylene exposures, e.g., more than 20 min. Defects including island edges, domain boundaries, and wrinkles are present in the graphene overlayers (Fig. S1) (23, 33–35).

CO adsorption on the graphene/Pt(111) surfaces at room temperature was investigated by polarization-modulation infrared reflection absorption spectroscopy (PM-IRRAS). Fig. 1*A* shows pressure-dependent PM-IRRAS spectra of CO adsorption on a 0.5 monolayer (ML) graphene on Pt(111) [0.5 ML Gr/Pt(111)]. Each spectrum was recorded in ultrahigh vacuum (UHV) after

Significance

Carbon deposits have been widely observed on metal surfaces in a variety of catalytic reactions, and the graphitic carbon species are often considered as inhibitors for surface reactions. We demonstrate here that CO adsorption and oxidation can occur on Pt surface covered by monolayer graphene, showing that the space between graphene overlayer and metal surface can act as a two-dimensional (2D) nanoreactor. Inside, CO oxidation happens with lower activation barrier due to the confinement effect of the graphene cover. This finding reminds us to reconsider the role of graphitic carbon in metal-catalyzed surface reactions and further provides a way to design novel catalysts.

Author contributions: Q.F. and X.B. designed research; Y.Y., Q.F., Y.Y.Z., X.W., H.L., M.C., L.J., R.M., P.J., H.B., Z.L., and S.B.Z. performed research; Y.Y., Q.F., Y.Y.Z., X.W., H.L., M.C., L.J., A.D., R.M., L.L., H.B., Z.L., S.B.Z., and X.B. analyzed data; and Y.Y., Q.F., Y.Y.Z., and X.B. wrote the paper.

The authors declare no conflict of interest.

This article is a PNAS Direct Submission.

[1]To whom correspondence should be addressed. Email: qfu@dicp.ac.cn.

This article contains supporting information online at www.pnas.org/lookup/suppl/doi:10.1073/pnas.1416368111/-/DCSupplemental.

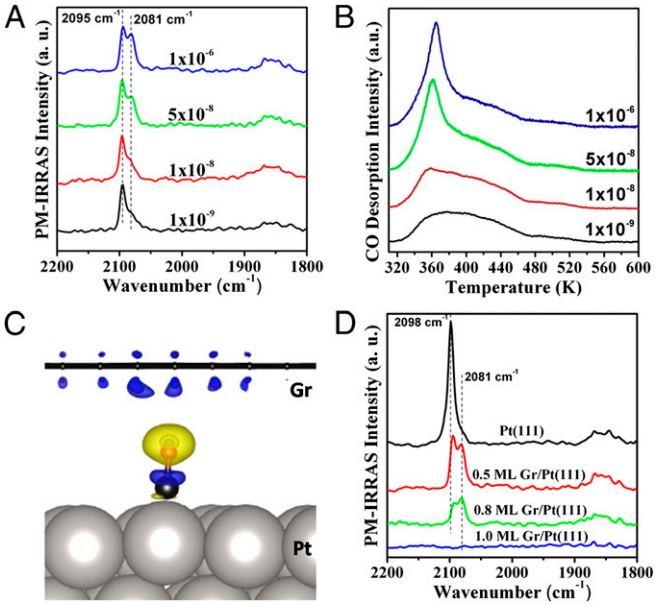

Fig. 1. CO PM-IRRAS (*A*) and CO-TPD (*B*) spectra acquired from the 0.5 ML Gr/Pt(111) surface exposed to CO at various pressures (Torr) at room temperature. Each IR and TPD spectrum was recorded after 10 min of CO exposure at the indicated pressure with subsequent evacuation to UHV. (*C*) Electron density difference of CO adsorbed at the Gr/Pt(111) interface. Black balls: C; red balls: O. Blue and yellow surfaces in the electron density difference are for electron depletion and electron accumulation, respectively. (*D*) CO PM-IRRAS from Pt(111), 0.5 ML Gr/Pt(111), 0.8 ML Gr/Pt(111), and 1 ML Gr/Pt(111) surfaces exposed to 1×10^{-6} Torr CO for 10 min at room temperature.

a 10-min CO exposure at the given CO pressure. The peak observed at 2,095 cm^{-1} is typical for the stretching vibration of CO adsorbed at the top sites of Pt(111), and the weaker broad peak around 1,850 cm^{-1} is due to CO adsorbed at the bridge sites of Pt(111) (36, 37). As the CO exposure pressure rose from 1×10^{-9} to 1×10^{-6} Torr, a new peak centered at 2,081 cm^{-1} appeared and its intensity was increased substantially with the CO pressure, becoming almost comparable to that of the peak at 2,095 cm^{-1} after 1×10^{-6} Torr CO exposure. In comparison, PM-IRRAS study of CO adsorption on the bare Pt(111) surface showed the only peak around 2,095 cm^{-1} even after an extended CO exposure in 1×10^{-6} Torr CO (Fig. S2*A*). Because CO does not adsorb on graphene overlayers grown on TMs at room temperature (38), the newly appeared peak at 2,081 cm^{-1} can be attributed to CO adsorbed on the top sites of Pt(111) but under the graphene overlayer [Gr/CO/Pt(111)]. The red shift of the C–O stretching frequency by 14 cm^{-1} compared with that on the bare Pt(111) surface underlines the confinement effect exerted by the graphene overlayer on the CO adsorption. In a recent work, similar IR study has been performed to probe CO adsorption on Ru(0001) under the confinement of a single-layer SiO_2 membrane (39).

CO intercalation at the Gr/Pt(111) interface was also studied by temperature-programmed desorption (TPD). After exposing the 0.5 ML Gr/Pt(111) surface to 1×10^{-9} Torr CO for 10 min at room temperature, the acquired CO TPD spectrum showed a broad desorption peak between 320 and 550 K (Fig. 1*B*), and its shape is similar to that of CO desorption from the bare Pt(111) surface (Fig. S2*B*). With an increase of the CO exposure pressure to 1×10^{-8} Torr, a new sharp CO desorption peak appeared at 360 K. Its intensity increased significantly and its position shifted to 365 K after a 1×10^{-6} Torr CO exposure. In contrast, both intensity and shape of the CO-TPD peak from the CO-saturated Pt(111) surfaces remain almost unchanged after exposure to various CO pressures (Fig. S2*B*). Similar to the pressure-dependent PM-IRRAS results, we suggest that the newly appeared TPD peak around 360 K upon exposing the surface to high pressure CO (>10^{-8} Torr) should be from CO desorption under the graphene overlayer, which happens intensively and quickly.

Both PM-IRRAS and TPD data reveal a significant effect of the graphene overlayer on the interaction of CO with Pt: (*i*) a red shift of the C–O stretching frequency; (*ii*) a sharp CO desorption at a lower temperature. To reveal the origin of the graphene effect, density functional theory (DFT) calculations were performed using $\sqrt{7} \times \sqrt{7}$ supercells for both Pt(111) and Gr/Pt(111) surfaces (Fig. S3). At the CO coverage of 3/7 ML, which is comparable with the experimental conditions, adsorption energy of CO on the top site of a bare Pt(111) surface is 1.74 eV, which decreases to 1.21 eV in the presence of graphene overlayers. The decrease in the adsorption energy of CO at the Gr/Pt interface is due to the energy penalty caused by lifting up the graphene overlayer. Our phonon calculation shows that CO stretching mode is 2,063 cm^{-1} on the bare Pt(111) surface while the mode decreases to 2,027 cm^{-1} at the Gr/Pt(111) interface. Qualitatively, the calculated red shift of CO stretching mode due to the existence of the graphene overlayer is consistent with our IR data. Using 1/7 ML CO adsorbed at the Gr/Pt(111) interface as a simple model, we plotted the electron density difference at the Gr/CO/Pt interface, as shown in Fig. 1*C*. Electronic interaction between graphene and CO molecule leads to an electron loss in the bond between C and O, which contributes to the weakened C–O bonding.

The CO adsorption on the Gr/Pt(111) surfaces with various graphene coverages was also studied by PM-IRRAS and TPD. After exposure of the bare Pt(111) surface to 1×10^{-6} Torr CO for 10 min, there is only one on-top CO vibrational peak around 2,098 cm^{-1}. On the 0.5 ML Gr/Pt(111) and 0.8 ML Gr/Pt(111) surfaces, this peak slightly shifts to 2,095 cm^{-1} due to the presence of surface graphene sheets. At the same time, an additional linear CO peak appears at 2,081 cm^{-1}, whose relative intensity grows with the increasing graphene coverage (Fig. 1*D*). As discussed above, this peak has been attributed to the stretching vibration of CO intercalated at the Gr/Pt(111) interface. It should be noted that the CO vibrational peak intensity became lower at the 0.8 ML Gr/Pt(111) surface, and not any CO adsorption signal was detected on the 1 ML Gr/Pt(111) surface. The CO TPD results also show that no CO uptake was observed on the 1 ML Gr/Pt(111) surface (Fig. S4). The results indicate that CO intercalation may be kinetically limited in the case of high coverage of graphene overlayer. Taken with the fact that CO intercalation has not been observed at the full graphene surface under high vacuum condition (<10^{-6} Torr), higher CO exposure pressure is needed to study any possible CO adsorption on the surface.

In the following, surface science techniques that can operate at near-ambient pressures are used to study CO adsorption under high-pressure atmosphere conditions. First, in situ PM-IRRAS was applied to monitor the 1 ML Gr/Pt(111) surface under CO pressures varying from 1×10^{-6} to 5 Torr (Fig. 2 *A* and *B*). Little CO adsorption was observed with CO pressure below 1×10^{-4} Torr. The CO adsorption peak at 2,081 cm^{-1}, characteristic of intercalated CO adsorbed at the top sites of Pt under the graphene cover (Gr/CO/Pt), emerged when the CO pressure increased to 1×10^{-4} Torr. The peak intensities increase with the CO pressures, which get saturated under 0.5 Torr CO. The absence of the 2,095 cm^{-1} peak regarding the on-top CO on bare Pt(111) [CO/Pt(111)] indicates that all of the surface CO molecules are under the graphene overlayer. Note that, at room temperature, most intercalated CO molecules can be kept under the graphene overlayer after evacuating the CO background. Temperature-dependent PM-IRRAS measurements of the Gr/CO/Pt(111) and CO/Pt(111) surfaces demonstrate that CO desorption from the 1 ML Gr/CO/Pt(111) surface occurs at a much lower temperature than that on the CO/Pt(111) surface, which again

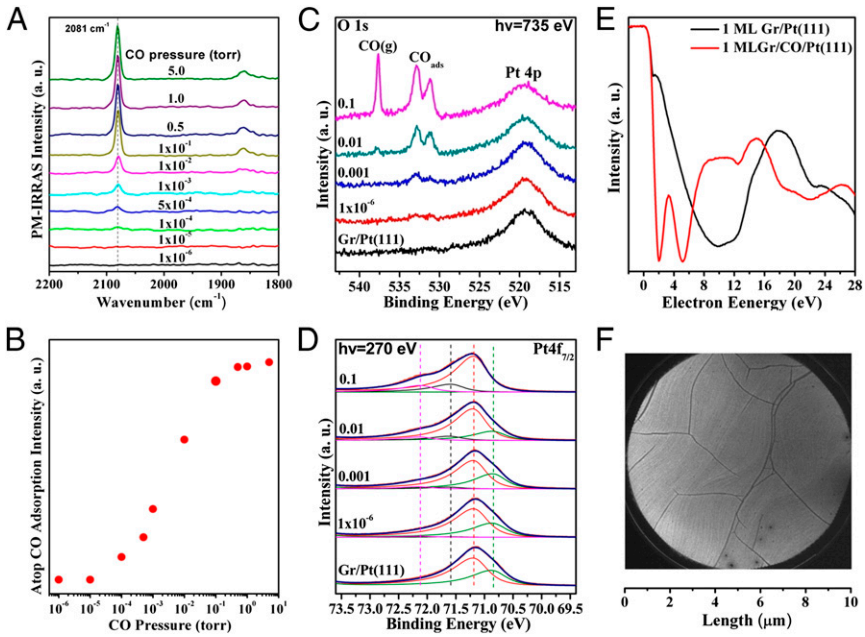

Fig. 2. CO intercalation under the full monolayer graphene overlayer. (*A*) In situ CO PM-IRRAS study in CO adsorption on the 1 ML Gr/Pt(111) surface at various CO pressures. (*B*) Dependence of the on-top CO adsorption intensity as a function of CO pressure. In situ ambient pressure XPS O 1s (*C*) and Pt $4f_{7/2}$ (*D*) spectra from the 1 ML Gr/Pt(111) surface exposed to UHV, 1×10^{-6}, 0.001, 0.01, and 0.1 Torr CO, respectively. The Pt $4f_{7/2}$ peaks can be deconvoluted into surface component, bulk component, and Pt species bonded with CO, which are all marked by dashed lines. (*E*) *I–V* curves and (*F*) LEEM image of the CO-intercalated Gr/Pt(111) surface. The 1 ML Gr/Pt(111) surface was exposed to CO atmosphere close to 1 bar in a high-pressure cell attached to the UHV-LEEM system, and then transferred to the UHV chamber for LEEM imaging.

confirms the weakened CO adsorption on Pt due to the confinement effect of the graphene overlayer (Fig. S5).

CO intercalation on the 1 ML Gr/Pt(111) surface was also investigated by in situ ambient pressure X-ray photoelectron spectroscopy (AP-XPS). O1s spectra show that there was little CO adsorption on the 1 ML Gr/Pt(111) surface in 1×10^{-6} Torr CO (Fig. 2*C*), whereas the bare Pt(111) surface has been almost saturated upon the same exposure to 1×10^{-6} Torr CO (Fig. S6*A*). At above 0.01 Torr CO, two strong O 1s peaks at 531.1 and 532.8 eV were observed on the 1 ML Gr/Pt(111) surface, which are attributed to the bridge and on-top CO on Pt(111), respectively (40). Meanwhile, the gas phase CO signals at 537.6 eV were detected (41). High-resolution XPS Pt $4f_{7/2}$ peak from a bare Pt(111) surface consists of a main component at 71.20 eV from the bulk Pt and a shoulder peak at 0.37 eV lower corresponding to the surface Pt component (Fig. S6*B*) (40). The surface component remains unchanged after being covered by one layer graphene because of the weak interaction between graphene overlayers and metal surfaces (24, 42, 43). However, a strong decrease of the surface Pt component was observed when the CO pressure was increased to above 0.01 Torr, and simultaneously two new peaks at 72.13 and 71.60 eV from surface Pt atoms bonded to CO appeared (40) (Fig. 2*D*). The O 1s and Pt 4f data clearly confirm that CO molecules adsorb between the graphene overlayer and the Pt surface in high-pressure CO atmosphere. Accompanied with these changes in the O 1s and Pt 4f signals, the binding energy of C 1s was also found shifted by −0.2 eV owing to decoupling of the graphene carbon atoms from the metal surfaces by the intercalated molecules (Fig. S7) (24, 25). The CO-intercalated graphene surface obtained by exposing the 1 ML Gr/Pt(111) surface to 1 bar CO was also imaged by LEEM (Fig. 2 *E* and *F*). There are two intensity minima at 2.0 and 5.2 eV in the intensity vs. electron energy (*I–V*) curve, which have been attributed to the intercalation-induced structural change at the graphene–metal interface (23). At the same time, the homogeneous LEEM image indicates that the CO intercalation takes place evenly under the whole graphene overlayer.

Overall, the high-pressure surface science investigations have shown that CO molecules can diffuse under the full graphene layer grown on Pt with CO pressure above 10^{-4} Torr. Obviously, the CO pressure needed for CO intercalation at the full monolayer graphene surface is much higher than that on the submonolayer graphene surface. On the full graphene layers grown on metal surfaces via chemical vapor deposition (CVD), it has been argued that diffusion of molecule species into graphene/metal interfaces happens through grain boundaries or pinholes (25, 31, 32), in contrast to the open edges of graphene islands on the submonolayer graphene. Molecule diffusion through the defects such as heptagons and octagons in the grain boundary needs a higher barrier compared with the same process through the island edges (30, 31, 44), which may be attributed to the observed higher CO pressure to intercalate the full graphene layer.

In addition, oxygen intercalation at the 1 ML Gr/Pt(111) surface were investigated by in situ AP-XPS. XPS O 1s, Pt 4f, and C 1s spectra confirm the oxygen intercalation at the 1 ML Gr/Pt(111) surface in 0.1 Torr O_2 and above 373 K (Fig. S8). These findings suggest that small molecules such as CO, O_2, and H_2 are prone to diffuse to the graphene/Pt interface under near-ambient conditions, which contrasts with the conventional knowledge that the full graphene overlayers act as a gas-impermeable coating on metal surfaces (45, 46).

Having shown that various gases can diffuse under the graphene overlayers, we suggest that the interface between the graphene overlayer and the Pt(111) surface can be used as a 2D nanoreactor for certain reactions. As an illustration, CO oxidation under the graphene overlayer was attempted at the Gr/Pt(111) interface. For comparison, the catalytic reactions were tested over the bare Pt(111) surface and the Gr/Pt(111) surfaces, with the mixture gases of 20 Torr CO and 10 Torr O_2 in a batch reactor. In situ PM-IRRAS was used to monitor the surface species during reactions,

while measuring the reaction kinetics simultaneously by recording the change of total pressures over time (47).

Fig. 3*A* shows Arrhenius plots of CO_2 formation rate over individual surfaces between 525 and 625 K. At 525 K, the Gr/Pt(111) surfaces present higher CO_2 formation rate than the clean Pt(111) surface. Above 525 K, the reaction rate sequence has been reversed with the highest rate observed on the Pt(111) surface. Nevertheless, the Gr/Pt(111) surfaces still maintain a relatively high CO formation rate. For example, the CO_2 formation rates at 600 K are 3.30×10^{16} molecule/s on the Pt(111) surface, 2.75×10^{16} molecule/s on the 0.5 ML Gr/Pt(111) surface, and 2.20×10^{16} molecule/s on the 1 ML Gr/Pt(111) surface. Assuming that all of the surface Pt atoms (around 1.5×10^{15} Pt atoms) are active in this reaction, the corresponding turnover frequencies (TOFs) (CO_2 molecules·site^{-1}·s^{-1}) at 600 K are 22.0, 18.3, and 14.7 on the three surfaces, respectively, which are consistent with literature results that TOFs of CO oxidation on Pt surfaces at 600 K vary from 10 to 80 depending on reaction gas pressures and gas compositions (48, 49). The apparent reaction activation energy can be derived from the Arrhenius plots of the CO_2 formation rate versus inverse reaction temperature (Fig. 3*A*), which yield 0.74 eV for the Pt(111) surface, 0.69 eV for 0.5 ML Gr/Pt(111), and 0.56 eV for the 1 ML Gr/Pt(111) surface. Note that the apparent reaction activation energy for CO oxidation on Pt(111) has been experimentally measured from 0.47 to 1. 8 eV (50–52), and our value is within this range.

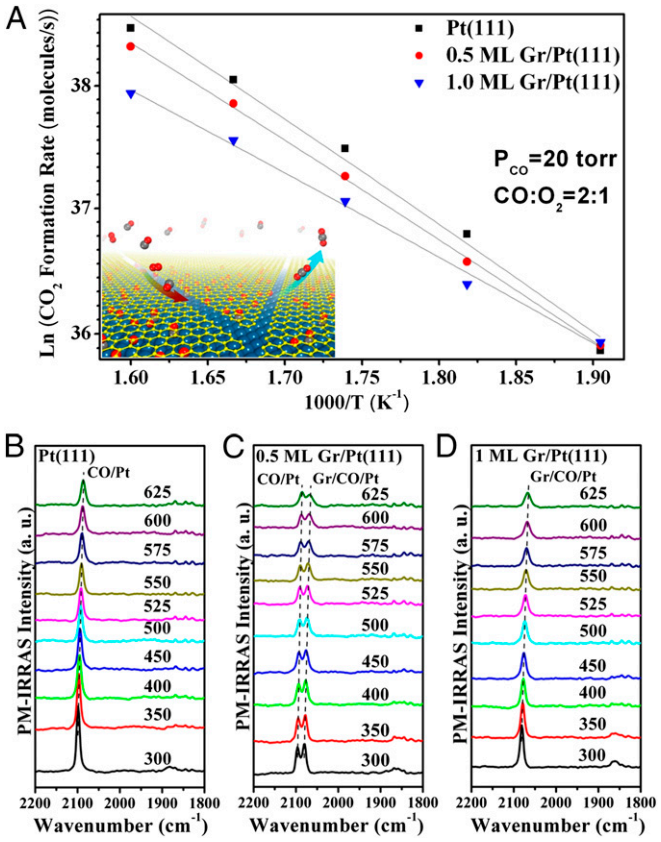

Fig. 3. CO oxidation at Pt(111) and Gr/Pt(111) surfaces. (*A*) Arrhenius plots of CO_2 formation rate on the Pt(111) surface and the Gr/Pt(111) surfaces in the temperature range of 525–625 K. The reaction gas consists of 20 Torr CO and 10 Torr O_2. The *Inset* schematically illustrates the simultaneous intercalation of CO and O_2 molecules underneath graphene flakes through the domain boundaries and the release of CO_2 from the interface. In situ CO PM-IRRAS spectra acquired from the Pt(111) (*B*), 0.5 ML Gr/Pt(111) (*C*), and 1 ML Gr/Pt(111) (*D*) surfaces in 30 Torr CO/O_2 (2:1) at the indicated reaction temperatures.

The reaction process can be better understood by taking advantage of in situ CO PM-IRRAS measurements during the reactions (Fig. 3 *B*–*D*). On the Pt(111) surface, only one vibrational peak at 2,098 cm^{-1} was detected in the linear band region under 30 Torr CO/O_2 (2:1) mixture at 300 K. This peak gradually shifts to lower frequency position and has smaller intensity with the increasing reaction temperature because the CO coverage decreases at the elevated temperatures (Fig. 3*B*). Both 2,095 and 2,081 cm^{-1} peaks are present in the spectra acquired from the 0.5 ML Gr/Pt(111) surface during all of the reaction process (Fig. 3*C*). On the 1 ML Gr/Pt(111) surface, only the vibrational peak at 2,081 cm^{-1} from on-top CO under graphene was observed at 300 K, which shifts to 2,067 cm^{-1} at 625 K (Fig. 3*D*). The absence of any signals from CO adsorbed on the bare Pt(111) surface indicates that the full graphene overlayer has been well kept during the CO oxidation process. The CO PM-IRRAS and Auger electron spectroscopy (AES) data before and after the reaction also show that the graphene overlayer is stable under the present applied reaction conditions, excluding the possibility of graphene oxidation by O_2 (Fig. S9).

Our reaction data demonstrate that the CO oxidation has been slightly enhanced on the Pt surfaces covered by graphene sheets at low temperature, e.g., 525 K. Considering that CO adsorption on Pt has been weakened by the graphene cover, we infer that the CO poisoning effect on Pt is alleviated at low temperatures, and, consequently, the CO oxidation has been facilitated. At high temperatures, the CO poisoning effect is not very critical, and, moreover, CO oxidation occurring under graphene sheets needs overcome barriers for molecule diffusion through the defects. Therefore, the CO_2 formation rate becomes lower over the Gr/Pt surfaces. Another interesting finding is that the Pt surface covered by the full graphene overlayer still presents quite high TOF. In situ PM-IRRAS spectra from the 1 ML Gr/Pt(111) surface show that, under the reaction conditions, surface-adsorbed CO molecules are all located underneath the graphene overlayer (Fig. 3*D*). Accordingly, the surface reactions should happen at the space between the graphene overlayer and the Pt(111) surface, in which both CO and O_2 diffuse inside and formed CO_2 products leave from the interface (Fig. 3*A*, *Inset*). This result confirms our hypothesis on the 2D nanoreactor under the graphene cover. It should be noted that the back face and side face of the Pt(111) single crystal can be coated by graphene overlayers in a similar way as the front face in our CVD process. Nevertheless, surface science measurements can only be carried out on the well-defined (111) front surface.

To better explain the experimental observations, CO oxidation at the Gr/Pt(111) interface was studied by DFT calculations. Under a CO preadsorption condition, adsorption energy of O atom on Pt(111) is around 1.08 eV. The big difference between the adsorption energies of CO (1.74 eV) and O on Pt(111) results in the well-known CO poisoning effect (53, 54). In the presence of graphene overlayers, the adsorption energy of O atom with CO preadsorption is not influenced, as the distance between O atoms and graphene overlayer is larger than 4 Å. The adsorption energies of O (1.08 eV) and CO (1.21 eV) are now comparable, which helps to alleviate the CO poisoning effect.

For calculation of the reaction barrier of CO oxidation on Pt (111) and Gr/Pt(111) surfaces, a 2/7 ML CO coverage is used, in which CO adsorption is considered at the top site and adsorption of O atom is considered at the hexagonal close-packed hollow site. In this model, one CO molecule reacts with O atom, and the other CO molecule plays the role to support graphene overlayer, to be comparable with experimental condition. It is well documented that CO oxidation on Pt below the CO ignition temperature is a Langmuir–Hinshelwood reaction between absorbed CO and O atoms (48, 52). We use climbing-image nudged elastic band method to investigate the reaction process, which already proves its validity in this reaction (55, 56). Six interstitial configurations

are used in between the starting configuration and the final configuration. Initial states (IS), transition states (TS), and final states (FS) are shown in Fig. S3. The presence of the graphene overlayer does not change the reaction path such that the TS configurations for both Pt(111) and Gr/Pt(111) cases are similar. Energy profiles for CO oxidation at the two surfaces are given in Fig. 4*A*. The reaction energy barrier on the bare Pt(111) surface is 0.66 eV, which is comparable with the values reported in previous literature (54, 56). On the Gr/Pt(111) surface, the energy barrier is 0.51 eV. Comparing with the bare Pt(111), the existence of graphene overlayer decreases the binding between molecules and substrate (a lift up of the energy profile in Fig. 4*A*) and we expect a flatter potential energy surface in the reaction path and thus a smaller reaction barrier.

To understand the role of graphene overlayer in the reaction, we calculated the electron density difference with atomic configuration fixed at the transition state. Isosurfaces of the electron density difference between the graphene overlayer and the remaining part are given in Fig. 4*B*. We can see that the electron depletion mainly occurs at two sites: one is the graphene overlayer (especially the carbon atoms right above the CO molecule), and the other is in the original C–O bond. On the other hand, electrons accumulate at the O atom and the newly formed C–O bond. Considering that electron accumulation is essential for the bond formation between the C atom in CO and the adsorbed O atom, the graphene-induced electron accumulation should decrease the reaction barrier. Electron density difference analysis indicates that the charge transfer from graphene to CO/O adsorbates weakens the origin C–O bond and promotes the formation of the second O–CO bond.

In summary, our results show that CO adsorption as well as CO oxidation can happen between graphene overlayer and Pt(111) surface. Weakened CO interaction with Pt under the graphene overlayer was identified with a lower desorption temperature and a red shift of CO stretching frequency compared with those on the bare Pt(111) surface. Moreover, a lower reaction barrier for CO oxidation under the graphene cover was observed than that over the bare Pt(111) surface. The electronic interaction between the top graphene overlayer and CO molecules underneath helps to weaken the C–O bond in CO and promote the formation of O–CO bond. The present results reveal that the graphene cover can exhibit a strong confinement effect on surface reactions on metals and enhance the metal-catalyzed reactions. We believe that the 2D confinement effect can be applied to metal-catalyzed reactions under other graphene-like covers, such as BN, 2D chalcogenides, and 2D oxides.

Methods

TPD and IRRAS. A stainless-steel UHV system coupled with a high-pressure/IR cell at the bottom was used for TPD, IRRAS, and reaction kinetics measurements. CO oxidation reaction was conducted in the high-pressure/IR cell (1.2 L in volume) in 30 Torr CO/O_2 (2:1) mixture. CO_2 formation rate was monitored using a baratron manometer where the reaction rate was derived from the pressure change of the reaction gas mixture. In situ CO IRRAS was recorded during the kinetics data measurements. A linear ramp of 3 K/s was used for TPD measurements. The Pt(111) sample was cleaned by repeated cycles of Ar^+ bombardment, heating in 1×10^{-6} Torr O_2 at 1,000 K, and annealing in UHV at 1,200 K until no contamination was detected by Auger electron spectroscopy. Graphene overlayers were grown on the Pt surface by CVD, which is exposure of the Pt(111) crystal to 10^{-7} Torr range ethylene at 950 K. The used graphene overlayers can be burned in O_2 and were reproduced by exposing to ethylene. High-purity CO and O_2 were further purified by passing through a liquid nitrogen (LN_2) cooling trap.

AP-XPS. AP-XPS measurements were performed at beamline 11.0.2 at the Advanced Light Source, Berkeley, with a specially designed photoemission spectrometer that can operate at near-ambient pressures (up to 2 Torr) (57, 58). Graphene overlayers were grown on the clean Pt(111) by the similar CVD process and the graphene coverage was measured by CO titration. High-purity CO was leaked into the UHV chamber through a leak valve. Once the CO pressure has been reached, Pt 4f spectra were acquired using a photon energy of 270 eV, C 1s spectra using 485 eV photon, and O 1s spectra using 735 eV photons. The Fermi edges measured at each of the photon energies were used for binding energy calibration. Beam damage was investigated by changing sample positions and checking for differences in the spectra. For CO and H_2 adsorption, the beam damage has been observed to be minimal. In O_2 adsorption, all spectra were always recorded from a fresh location on the sample surface immediately after opening the shutter for the X-ray beam.

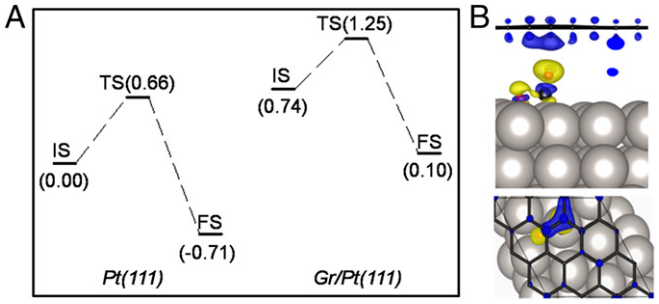

Fig. 4. DFT calculations of CO oxidation on Pt(111) with or without graphene. (*A*) Calculated reaction barriers for oxidation between CO and O on Pt(111) and Gr/Pt(111), respectively. Values in the brackets are in unit of electron volt. (*B*) Electron density difference of the transition state at the Gr/Pt(111) interface. Black balls: carbon; red balls: oxygen. Blue and yellow surfaces in the electron density difference are for electron depletion and electron accumulation, respectively.

DFT Calculation. First-principles calculations were carried out based on DFT, projector augmented waves, and a plane wave basis set as implemented in the Vienna ab initio simulation package (VASP). Exchange-correlation effects are modeled using Perdew–Burke–Ernzerh functional (PBE) with corrections for the missing dispersion forces in the form of C^6/R^6 pair potentials (PBE-D). C^6 for Pt is chosen as 24.67 $J{\cdot}nm^6{\cdot}mol^{-1}$, and van der Waals (vdW) radius, R^{vdW}, is chosen to be 1.75 Å. This set of parameters give a graphene-Pt(111) distance of 3.3 Å, which is comparable with experiments. A $\sqrt{7} \times \sqrt{7}$ Pt(111) supercell with four Pt layers slab model was used to model the CO oxidation process. Comparing with a 3×3 graphene supercell, there is a 0.6% lattice mismatch. Plane waves with cutoff energy at 400 eV were used as the basis set. Monkhorst–Pack $3 \times 3 \times 1$ k-point grid was used to sample the Brillouin zone. In structural relaxations, all atoms except for the bottom two Pt layers were fully relaxed until the forces are smaller than 0.01 eV/Å.

ACKNOWLEDGMENTS. We thank the fruitful discussions with Dr. Fan Yang. This work was financially supported by the National Natural Science Foundation of China (Grants 21222305, 21373208, and 21033009), Ministry of Science and Technology of China (Grants 2011CB932704 and 2013CB834603), and the Key Research Program of the Chinese Academy of Sciences. The work at Texas A&M University was supported by the US Department of Energy (DOE), Office of Basic Energy Sciences, Division of Chemical Sciences, Geosciences, and Biosciences (Grant DE-FG02-95ER-14511). Y.Y.Z. and S.B.Z. were supported by the US DOE, Office of Basic Energy Sciences (Grant DE-SC0002623). The supercomputer time was provided by National Energy Research Scientific Computing Center under Grant DE-AC02-05CH11231; the Extreme Science and Engineering Discovery Environment Science Gateways Program, which is supported by National Science Foundation Grant ACI-1053575; and Center for Computational Innovations at Rensselaer Polytechnic Institute. The Advanced Light Source and beamline 11.0.2 are supported by the Director, Office of Energy Research, Office of Basic Energy Sciences, and Chemical Sciences Division of the US DOE under Contracts DE-AC02-05CH11231.

1. Schlögl R (2008) Carbons. In *Handbook of Heterogeneous Catalysis*, eds Ertl G, Knözinger H, Schüth F, Weitkamp J (Wiley-VCH, Weinheim, Germany), Vol 1, pp 357–427.
2. Goodman DW, Kelley RD, Madey TE, Yates JTJ (1980) Kinetics of the hydrogenation of CO over a single crystal nickel catalyst. *J Catal* 63(1):226–234.
3. Davis SM, Zaera F, Somorjai GA (1982) The reactivity and composition of strongly adsorbed carbonaceous deposits on platinum. Model of the working hydrocarbon coversion catalyst. *J Catal* 77(2):439–459.
4. Webb G (1990) The formation and role of carbonaceous residues in metal-catalysed reactions of hydrocarbons. *Catal Today* 7(2):139–155.

5. Brandt B, et al. (2008) Isomerization and hydrogenation of *cis*-2-butene on Pd model catalyst. *J Phys Chem C* 112(30):11408–11420.
6. Wolf EE, Alfani F (1982) Catalyst deactivation by coking. *Catal Rev Sci Eng* 24(3):329–371.
7. Bartholomew CH (2001) Mechanisms of catalyst deactivation. *Appl Catal A Gen* 212(1-2):17–60.
8. Peng Z, et al. (2012) High-resolution in situ and ex situ TEM studies on graphene formation and growth on Pt nanoparticles. *J Catal* 286:22–29.
9. Besenbacher F, et al. (1998) Design of a surface alloy catalyst for steam reforming. *Science* 279(5358):1913–1915.
10. Lu J, et al. (2012) Coking- and sintering-resistant palladium catalysts achieved through atomic layer deposition. *Science* 335(6073):1205–1208.
11. Deng D, et al. (2013) Iron encapsulated within pod-like carbon nanotubes for oxygen reduction reaction. *Angew Chem Int Ed Engl* 52(1):371–375.
12. Wu G, More KL, Johnston CM, Zelenay P (2011) High-performance electrocatalysts for oxygen reduction derived from polyaniline, iron, and cobalt. *Science* 332(6028): 443–447.
13. Goodman DW, White JM (1979) Measurement of active carbon on ruthenium (110): Relevance to catalytic methanation. *Surf Sci* 90(1):201–203.
14. McCrea KR, Parker JS, Somorjai GA (2002) The role of carbon deposition from CO dissociation on platinum crystal surfaces during catalytic CO oxidation: Effects on turnover rate, ignition temperature, and vibrational spectra. *J Phys Chem B* 106(42): 10854–10863.
15. Aizawa T, et al. (1990) Photon dispersion in monolayer graphite formed on Ni(111) and Ni(001). *Surf Sci* 237(1-3):194–202.
16. Wu MC, Xu Q, Goodman DW (1994) Investigations of graphitic overlayers formed from methane decomposition on Ru(0001) and Rh(1120) catalysts with scanning tunneling microscopy and high resolution electron energy loss spectroscopy. *J Phys Chem* 98(19):5104–5110.
17. Land TA, Michely T, Behm RJ, Hemminger JC, Comas G (1991) STM investigation of the adsorption and temperature dependent reactions of ethylene on Pt(111). *Appl Phys A Mater Sci Process* 53(5):414–417.
18. Novoselov KS, et al. (2012) A roadmap for graphene. *Nature* 490(7419):192–200.
19. Wintterlin J, Bocquet M-L (2009) Graphene on metal surfaces. *Surf Sci* 603(10): 1841–1852.
20. Batzill M (2012) The surface science of graphene: Metal interfaces, CVD synthesis, nanoribbons, chemical modifications, and defects. *Surf Sci Rep* 67(3):83–115.
21. Zhang H, Fu Q, Cui Y, Tan DL, Bao XH (2009) Growth mechanism of graphene on Ru(0001) and O_2 adsorption on the graphene/Ru(0001) surface. *J Phys Chem C* 113(19): 8296–8301.
22. Sutter P, Sadowski JT, Sutter EA (2010) Chemistry under cover: Tuning metal-graphene interaction by reactive intercalation. *J Am Chem Soc* 132(23):8175–8179.
23. Mu R, et al. (2012) Visualizing chemical reactions confined under graphene. *Angew Chem Int Ed Engl* 51(20):4856–4859.
24. Grånäs E, et al. (2013) CO intercalation of graphene on Ir (111) in the millibar regime. *J Phys Chem C* 117(32):16438–16447.
25. Jin L, et al. (2014) Surface chemistry of CO on Ru (0001) under the confinement of graphene cover. *J Phys Chem C* 118(23):12391–12398.
26. Feng X, Maier S, Salmeron M (2012) Water splits epitaxial graphene and intercalates. *J Am Chem Soc* 134(12):5662–5668.
27. Gao L, et al. (2012) Repeated growth and bubbling transfer of graphene with millimetre-size single-crystal grains using platinum. *Nat Commun* 3:699.
28. Jin L, Fu Q, Yang Y, Bao X (2013) A comparative study of intercalation mechanism at graphene/Ru(0001) interface. *Surf Sci* 617:81–86.
29. Grånäs E, et al. (2012) Oxygen intercalation under graphene on Ir(111): Energetics, kinetics, and the role of graphene edges. *ACS Nano* 6(11):9951–9963.
30. Zhang X, Wang L, Xin J, Yakobson BI, Ding F (2014) Role of hydrogen in graphene chemical vapor deposition growth on a copper surface. *J Am Chem Soc* 136(8): 3040–3047.
31. Duong DL, et al. (2012) Probing graphene grain boundaries with optical microscopy. *Nature* 490(7419):235–239.
32. Hsieh Y-P, et al. (2014) Complete corrosion inhibition through graphene defect passivation. *ACS Nano* 8(1):443–448.
33. Zhang Y, et al. (2013) Enhanced reactivity of graphene wrinkles and their function as nanosized gas inlets for reactions under graphene. *Phys Chem Chem Phys* 15(43): 19042–19048.
34. Sutter P, Sadowski JT, Sutter E (2009) Graphene on Pt (111): Growth and substrate interaction. *Phys Rev B* 80(24):245411.
35. Yan Z, Peng Z, Tour JM (2014) Chemical vapor deposition of graphene single crystals. *Acc Chem Res* 47(4):1327–1337.
36. Andersen M, Johansson M, Chorkendorff I (2005) Isotopic exchange of CO adsorbed on Pt(111). *J Phys Chem B* 109(20):10285–10290.
37. Wadayama T, et al. (2008) Infrared reflection—absorption study of carbon monoxide adsorption on Fe/Pt (111) bimetallic surfaces. *J Phys Chem C* 112(24):8944–8950.
38. Liu L, et al. (2011) The 2-D growth of gold on single-layer graphene/Ru(0001): Enhancement of CO adsorption. *Surf Sci* 605(17):L47–L50.
39. Emmez E, Yang B, Shaikhutdinov S, Freund HJ (May 21, 2014) Permeation of a single-layer SiO_2 membrane and chemistry in confined space. *J Phys Chem C*, 10.1021/jp503253a.
40. Tao F, et al. (2010) Break-up of stepped platinum catalyst surfaces by high CO coverage. *Science* 327(5967):850–853.
41. Schnadt J, et al. (2012) The new ambient-pressure X-ray photoelectron spectroscopy instrument at MAX-lab. *J Synchrotron Radiat* 19(Pt 5):701–704.
42. Preobrajenski A, Ng ML, Vinogradov A, Mårtensson N (2008) Controlling graphene corrugation on lattice-mismatched substrates. *Phys Rev B* 78(7):073401.
43. Larciprete R, et al. (2012) Oxygen switching of the epitaxial graphene-metal interaction. *ACS Nano* 6(11):9551–9558.
44. Nilsson L, Andersen M, Hammer B, Stensgaard I, Hornekær L (2013) Breakdown of the graphene coating effect under sequential exposure to O_2 and H_2S. *J Phys Chem Lett* 4(21):3770–3774.
45. Chen S, et al. (2011) Oxidation resistance of graphene-coated Cu and Cu/Ni alloy. *ACS Nano* 5(2):1321–1327.
46. Prasai D, et al. (2012) Graphene: Corrosion-inhibiting coating. *ACS Nano* 6(2): 1102–1108.
47. Chen MS, Goodman DW (2004) The structure of catalytically active gold on titania. *Science* 306(5694):252–255.
48. Berlowitz PJ, Peden CH, Goodman DW (1988) Kinetics of carbon monoxide oxidation on single-crystal palladium, platinum, and iridium. *J Phys Chem* 92(18):5213–5221.
49. Joo SH, et al. (2009) Thermally stable Pt/mesoporous silica core-shell nanocatalysts for high-temperature reactions. *Nat Mater* 8(2):126–131.
50. Su X, Cremer PS, Shen YR, Somorjai GA (1997) High-pressure CO oxidation on Pt(111) monitored with infrared-visible sum frequency generation (SFG). *J Am Chem Soc* 119(17):3994–4000.
51. Farkas A, et al. (2013) High pressure carbon monoxide oxidation over platinum (111). *J Phys Chem C* 117(19):9932–9942.
52. Campbell C, Ertl G, Kuipers H, Segner J (1980) A molecular beam study of the catalytic oxidation of CO on a Pt (111) surface. *J Chem Phys* 73(11):5862–5873.
53. Bleakley K, Hu P (1999) A density functional theory study of the interaction between CO and O on a Pt Surface: CO/Pt (111), O/Pt (111), and CO/O/Pt (111). *J Am Chem Soc* 121(33):7644–7652.
54. Fu Q, et al. (2010) Interface-confined ferrous centers for catalytic oxidation. *Science* 328(5982):1141–1144.
55. Alavi A, Hu P, Deutsch T, Silvestrelli PL, Hutter J (1998) CO oxidation on Pt (111): An ab initio density functional theory study. *Phys Rev Lett* 80(16):3650–3653.
56. Eichler A, Hafner J (1999) Reaction channels for the catalytic oxidation of CO on Pt (111). *Phys Rev B* 59(8):5960–5967.
57. Bluhm H, et al. (2006) Soft X-ray microscopy and spectroscopy at the molecular environmental science beamline at the Advanced Light Source. *J Electron Spec Rel Phen* 150(2):86–104.
58. Salmeron M, Schlögl R (2008) Ambient pressure photoelectron spectroscopy: A new tool for surface science and nanotechnology. *Surf Sci Rep* 63(4):169–199.